

Indirect spin-orbit K splittings in strontium

J. Nunkaew, E. S. Shuman, and T. F. Gallagher

Department of Physics, University of Virginia, Charlottesville, Virginia 22904, USA

(Received 17 December 2008; published 4 May 2009)

We use delayed field ionization to observe the microwave resonance transitions of Sr from $5snf$ to $5sng$, $5snh$, and $5sni$. The energies of the $5sn\ell$, $\ell > 3$ states are split by the indirect spin-orbit coupling of the Sr core to the Rydberg electron, producing the K splittings. From the K splittings we extract the ionic dipole and quadrupole matrix elements, $\langle 5s|r|5p \rangle = 3.65(25)a_0$ and $\langle 5s|r^2|4d \rangle = 12(14)a_0^2$. From the dipole matrix element we obtain the dipole polarizability of Sr^+ . With the dipole polarizability and the quantum defect differences of adjacent l states, we can determine the Sr^+ quadrupole polarizability. The dipole and quadrupole polarizabilities of Sr^+ are $\alpha_d = 86(11)a_0^3$ and $\alpha_q = 1.1 \times 10^3(10)a_0^5$, respectively.

DOI: 10.1103/PhysRevA.79.054501

PACS number(s): 32.30.Bv, 32.80.Ee, 31.15.ap

It is well known that measuring the intervals between the high-angular momentum bound Rydberg states provides an excellent way of determining the dipole and quadrupole polarizabilities of the ionic core. However, it is less well known that the K splittings, or indirect spin-orbit splittings, of the high- ℓ states can be used to determine the dipole and quadrupole matrix elements connecting the ground state of the ion, typically an s state, to the lowest-lying p and d states [1]. These matrix elements are important in many contexts. For example, Sr^+ , which we consider here, is a candidate for atomic parity nonconservation (PNC) measurements [2], and an accurate $5s$ - $5p$ radial matrix element for Sr^+ is needed to precisely calculate the parity-violating amplitude. The ionic quadrupole matrix element determines the lifetime of the $4d$ state since the metastable $(n-1)d$ states of alkaline-earth-metal ions decay to the ns ground state by an electric quadrupole (E2) process [3]. Since this lifetime is long, 0.425 s [3], it is difficult to measure, but it is important since it determines the inherent linewidth of the atomic $5s$ - $4d$ quadrupole transition of the Sr^+ ion, a candidate for an optical frequency standard [4]. The oscillator strengths calculated from $5s$ - $5p$ and $5s$ - $4d$ matrix elements also have application in astrophysics in determining the solar abundance of strontium [5].

The best description for the bound high- ℓ $5snl$ Rydberg states of Sr is obtained by coupling the angular momentum of the ionic core, \vec{j}_i , to the orbital angular momentum of the Rydberg electron, \vec{l} , to form \vec{K} . Explicitly, $\vec{K} = \vec{j}_i + \vec{l}$, and for the bound $5snl$ Rydberg states $K = l \pm \frac{1}{2}$. We ignore the spin of the Rydberg electron, which when coupled to \vec{K} gives states of total angular momentum $J = K \pm \frac{1}{2}$. The K splitting arises because the value of K determines the strengths of the dipole and quadrupole couplings to the doubly excited states, such as the Sr $4d_jnd$ states. The contribution to the K splitting from an excited state of the ion is proportional to the square of the radial matrix element connecting the ground state to the excited state, the fine-structure splitting of the excited state, and the inverse cube of the excitation energy of the excited state. As a result, in Sr the K splittings are almost entirely determined by the lowest-lying $5p$ and $4d$ states of Sr^+ .

Here we report microwave resonance measurements of the Sr $5snf$ - $5sng$ - $5snh$ - $5sni$ intervals, including their K splittings. From the K splittings we derive the $5s$ - $5p$ and $5s$ - $4d$

radial matrix elements, and from the intervals between the ℓ states we derive a value for the quadrupole polarizability of Sr^+ . In this Brief Report we describe the experimental approach, our experimental observations, and the data analysis using the K splitting and core polarization models. We use atomic units, unless specified otherwise.

The core polarization and K splitting models are applicable to high- ℓ states in which there is no core penetration. With this idea in mind we have observed the Sr $5snf \rightarrow 5sng$, $5snf \rightarrow 5snh$, and $5snf \rightarrow 5sni$ transitions using a microwave resonance technique. Sr atoms in a beam pass into the interaction region between two plates where they are excited from the ground state, $5s5s \ ^1S_0$ to the $5s5p \ ^1P_1$, $5s5d \ ^1D_2$, and $5snf \ ^1F_3$ states using dye laser pulses of wavelengths 460.9, 767.5, and ~ 908 nm, respectively, as shown in Fig. 1. The last laser is tunable over the range of 908–920 nm to cover $n=18$ to $n=24$. Since the $5snf$ state is a singlet state, transitions from $5snf$ to a higher-angular momentum state $5snl$ should yield two resonant peaks due to the K splitting of $5snl$ states of $\ell > 3$. The splitting of the analogous K states has been previously reported for both Ba and Si^{2+} [6–8].

A microwave pulse 1 μs long is sent into the interaction region 10 ns after the last laser pulse to drive the $5snf$ - $5snl$ transition. We have detected the transition using delayed field ionization (DFI) [6]. A field pulse is applied 10–20 μs after

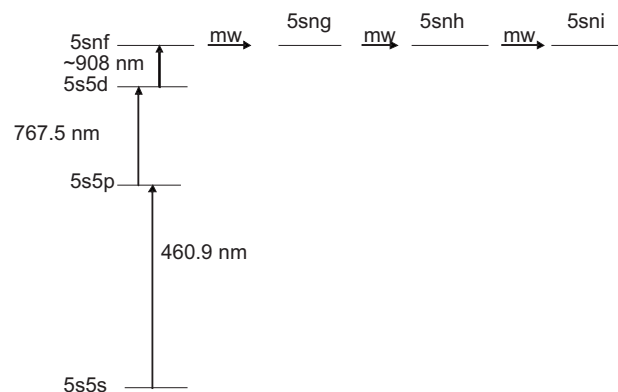


FIG. 1. Energy levels in this experiment. The vertical arrows represent the transitions driven by different wavelength dye lasers. The horizontal arrows represent the transitions driven by different microwave frequencies.

TABLE I. $nf-ng$ transition intervals.

n	$nf-ng$ $K=7/2$ (GHz)	$nf-ng$ $K=9/2$ (GHz)	ng K splitting (MHz)
20	37.3932(18)	37.9388(8)	545.6(20)
21	32.5104(12)	32.9736(10)	463.2(16)
22	28.4120(14)	28.8246(28)	412.6(32)
23	24.9574(38)	25.3310(30)	373.6(48)

the microwave pulse to field ionize all Rydberg atoms which live this long, and we detect the resulting electrons. The use of DFI to detect the resonant transitions is based on the fact that the higher-angular momentum states live longer than the $5snf$ states [6]. Hence when the microwave pulse drives the $5snf \rightarrow 5snl$ transition, the number of atoms living 10–20 μs increases substantially. It is easier to discriminate between the signals from different states this way than using selective field ionization (SFI).

The microwaves are generated by a Hewlett-Packard 8350B/83550A sweep oscillator, which operates between 8 and 20 GHz. The continuous-wave (cw) output of the oscillator is formed into 1 μs pulses using a microwave switch. The microwave frequency is doubled by a DBS 1826X220 (9–13.25 to 18–26.5 GHz) or a Phase One SX40-220 (13.25–20 to 26.5–40 GHz) active doubler. The doubled microwaves pass through a K or R band waveguide attenuator en route to a horn. Microwaves from the horn enter the interaction region by passing through a re-entrant Pyrex window in the vacuum chamber. A Systron Donner 6246A frequency counter is used to measure the frequency of the microwave source with an accuracy better than 0.1 MHz. The one- and two-photon transitions are driven by a single microwave field. To drive the three-photon $5snf-5sni$ transition, we use, in addition, a Hewlett-Packard 83620A synthesizer to produce a radio-frequency (rf) field with frequency

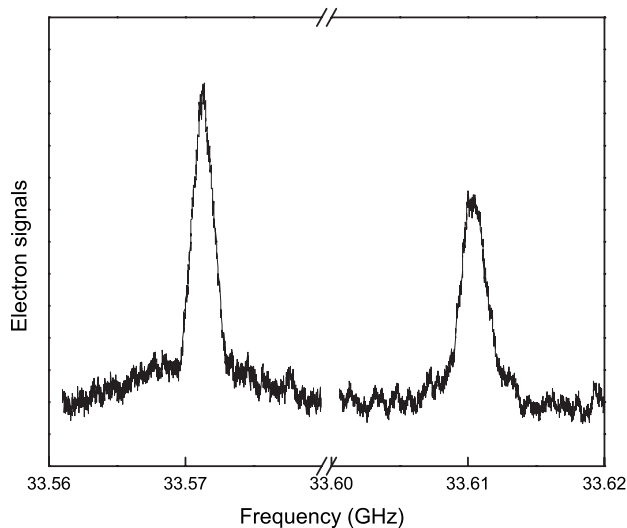


FIG. 2. Two-photon $5s19f \rightarrow 5s19h$ resonance. The relative microwave power of the first resonant peak is 0.32 and the relative microwave power of the second resonant peak is 0.40. Note that the interval is twice the measured frequency.

TABLE II. $nf-nh$ transition intervals.

n	$nf-nh$ $K=9/2$ (GHz)	$nf-nh$ $K=11/2$ (GHz)	nh K splitting (MHz)
18	78.4828(8)	78.5800(8)	97.2(11)
19	67.1424(6)	67.2204(6)	78.0(8)
20	57.8536(6)	57.9220(8)	68.4(10)
21	50.1892(8)	50.2504(10)	61.2(13)
22	43.8132(10)	43.8692(12)	56.0(16)

of ~ 5 GHz. The rf field enters the interaction region from a rf horn placed inside the vacuum chamber on the side of the interaction region opposite the microwave horn.

Optical spectroscopy of the Sr $5snf$ states provides a quantum defect for the $5snf \ ^1F_3$ series of $\delta_f=0.08$ [9]. Assuming that this quantum defect arises entirely from the dipole polarizability of the Sr^+ core, we estimate the Sr $5snf-5sng$ frequencies, in THz, to be given by $\nu \sim 526n^{-3}$, and we used this estimate to begin the search for the $5snf-5sng$ resonances. The one-photon $5snf-5sng$ transitions appear as two resonant peaks with approximately equal strengths as we expected. Power broadening is eliminated by attenuating the microwave power and, due to the earth's magnetic field, the minimum linewidth is ~ 4 MHz. The observed intervals are given in Table I.

Since the two-photon $5snf-5snh$ transitions exhibit an ac Stark shift, they are observed at different microwave powers and the intervals extrapolated to zero microwave power. For each $5snf-5snh$ transition, there are two equally strong resonant peaks as shown in Fig. 2. The observed intervals, extrapolated to zero microwave power, are given in Table II.

To drive the three-photon $5snf-5sni$ transition, we use one rf photon and two microwave photons. Using the additional rf frequency we can tune the microwave frequency close to the $nf-nh$ two-photon resonance and efficiently drive the three-photon transition. The rf frequency is kept constant while the microwave frequency is swept through the appropriate range. We again observe two resonant peaks, as expected. The sum of the rf frequency and twice the microwave frequency gives us the three-photon intervals. When the rf frequency is varied over a 30 MHz range, the resonant peaks occur at different microwave frequencies, but the sum of the rf and twice the microwave frequency is constant to within ~ 1 MHz. The rf and microwave powers are attenuated to account for the power shifts. Extrapolating the graphs of frequency vs relative power for both rf and microwave powers, we find that the larger power shift is that due to the microwave power, which can be as much as 10 MHz. The rf power

TABLE III. $nf-ni$ transition intervals.

n	$nf-ni$ $K=11/2$ (GHz)	$nf-ni$ $K=13/2$ (GHz)	ni K splitting (MHz)
20	64.3317(10)	64.3494(15)	17.7(18)
21	55.7904(24)	55.8062(12)	15.8(27)
22	48.6947(12)	48.7079(15)	13.2(19)

TABLE IV. γ_{5pnl} (10^{-10} a.u.).

n	$l=4$	$l=5$	$l=6$
18		9.96	
19		8.53	
20	36.8	7.37	1.95
21	31.9	6.40	1.70
22	27.8	5.60	1.49
23	24.4		

shift is always less than 1 MHz. Both the rf and microwave power shifts exhibit the expected linear dependence, and the observed intervals, extrapolated to zero microwave and rf power, are given in Table III.

To extract the ionic dipole and quadrupole matrix elements, we express the K splittings in terms of them. Explicitly,

$$K_{nl} = \langle 5s|r|5p \rangle^2 \gamma_{5snl} + \langle 5s|r^2|4d \rangle^2 \gamma_{4dnl}, \quad (1)$$

where γ_{5pnl} and γ_{4dnl} are as defined in Eqs. (39) and (40) of Shuman and Gallagher [1]. The factors γ_{5pnl} and γ_{4dnl} consist of radial matrix elements, angular factors, and energy differences, and are calculated numerically. The radial matrix elements $\langle nl|\frac{1}{r^2}|n'l' \rangle$ and $\langle nl|\frac{1}{r^3}|n'l' \rangle$ are calculated using a Numerov algorithm with hydrogen wave functions. The $n\ell$ energies are assumed to be hydrogenic and the Sr^+ energies are the known energies. The calculated values of γ_{5pnl} and γ_{4dnl} are given in units of 10^{-10} and 10^{-12} atomic units in Tables IV and V, respectively.

In Fig. 3 we show a plot of $\frac{K_{nl}}{\gamma_{5snl}}$ vs $\frac{\gamma_{4dnl}}{\gamma_{5snl}}$ using the $5sng$, $5snh$, and $5sni$ K splittings. The fit of the data to the broken line is, we believe, an artifact. The $5sng$ states are coupled to the $4dnd$ states, in which the outer nd electron is core penetrating and has nonzero quantum defect. For example, the $4d^2\ ^3P_2$ state lies at $44\ 729.6\ \text{cm}^{-1}$ [10]; i.e., it is bound by $1200\ \text{cm}^{-1}$. The energies of the $4d^2$ states of $J=3, 4,$ and 5 , which interact with the $5sng$ states, we observe to be unknown but presumably not far away. In contrast, the model we used is based on the assumption that the nd electron is hydrogenic, in which case the $4d^2$ state would be $8000\ \text{cm}^{-1}$ above the ionization limit, not $1200\ \text{cm}^{-1}$ below it. Not only are the $4dnd$ energies incorrect, but the $\langle ng|1/r^3|n'd \rangle$ matrix elements are as well. Since the $5sng$ states cannot be used in the analysis we fit only the $5snh$ and $5sni$ K splitting data,

TABLE V. γ_{4dnl} in 10^{-12} a.u.

n	$l=5$	$l=6$	
18		8.54	
19		7.38	
20	407	6.41	0.66
21	359	5.61	0.58
22	318	4.93	0.51
23	283		

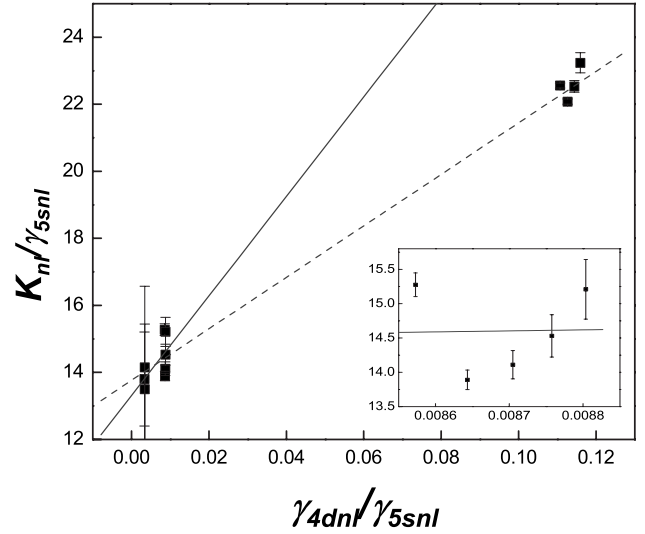


FIG. 3. Graph of $\frac{K_{nl}}{\gamma_{5snl}}$ vs $\frac{\gamma_{4dnl}}{\gamma_{5snl}}$. The broken line is fit to the $5sng$, $5snh$, and $5sni$ K splittings, and the solid line is fit to the $5snh$ and $5sni$ splittings, yielding slope of $|\langle 5s|r_1^2|4d \rangle|^2 = 1.5 \times 10^2(20)$ and y intercept of $|\langle 5s|r_1|5p \rangle|^2 = 13.3(18)$. The nh series of the graph, shown in the inset, shows the deviation of the $5snh$ data from the fit line.

yielding the solid line in Fig. 3, from which we obtain $\langle 5s|r^2|4d \rangle = 12(14)$ and $\langle 5s|r|5p \rangle = 3.65(25)$. In Table VI, we compare our results to other theoretical and experimental results. While our values are in reasonable agreement with other values, it is interesting to note that the n dependence of the $5snh$ and $5sng$ data points does not match the line of the l dependence, as shown by the inset of Fig. 3, which shows the $5snh$ data on an expanded scale. The discrepancy is larger than the experimental uncertainty and the estimated 1% uncertainty of the numerical calculations. The origin of this discrepancy is not understood.

Since only the $5snh$ and $5sni$ states are usable in a core polarization analysis, we obtain a value for the polarizabilities as follows. The contribution of the Sr^+ $5s$ - $5p$ transition to the dipole polarizability is $80(11)a_0^3$. Based on the oscillator strengths of Sr^+ [16], we estimate that higher- np states and the ϵp continuum add 0.3%. To these we add the polarizability of Sr^{2+} , $5.81 a_0^3$ [12,17], to arrive at $\alpha_d = 86(11)a_0^3$. Following a similar procedure we use the Sr^+ $5s$ - $5p$ matrix element of Gallagher [13] to calculate a dipole polarizability

TABLE VI. Ionic dipole and quadrupole matrix elements obtained from this work and other theoretical and experimental results [11,12].

$\langle 5s r_1 5p \rangle$	$\langle 5s r_1^2 4d \rangle$
3.65(25) ^a	12(14) ^a
3.73 ^b	12.42 ^b
3.78 ^c	12.27 ^d
3.78 ^e	12.24 ^f

^aPresent work.

^bReference [12].

^cReference [13].

^dReference [3].

^eReference [14].

^fReference [15].

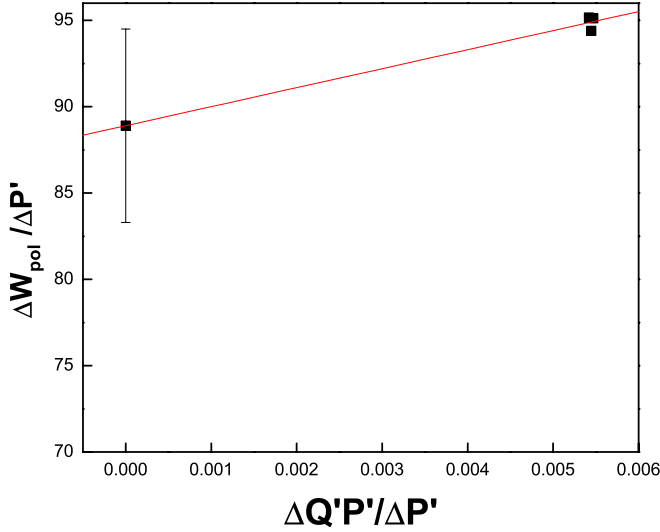


FIG. 4. (Color online) Graph of $\frac{\Delta W_{\text{pol}}}{\Delta P'}$ vs $\frac{\Delta P'Q'}{\Delta P'}$. The line represents the least-squares fit. The y intercept is our calculated α_d . The slope is $[1.1 \times 10^3(10)]a_0^5$.

$\alpha_d = 91.8(25)a_0^3$. Averaging these two values yields $\bar{\alpha}_d = 88.9(56)$. With this value of $\bar{\alpha}_d$ and the $5snh$ - $5sni$ intervals, we can obtain a value for α_q using

$$\frac{\Delta W_{\text{pol}}}{\Delta P'} = \alpha_d + \alpha_q \frac{\Delta P'Q'}{\Delta P'}, \quad (2)$$

where ΔW_{pol} is the interval between the $5sn\ell$ and $5sn\ell'$ states, and $\Delta P'$ and $\Delta P'Q'$ are as defined by Gallagher *et al.* [6] and Shuman and Gallagher [1]. They contain the non-adiabatic corrections. An alternative method of extracting the polarizabilities, the adiabatic expansion approach, was described by Snow and Lundeen [18]. A plot of Eq. (2) using the calculated value of $\bar{\alpha}_d$, which provides a point at $\Delta P'Q'/\Delta P' = 0$, and the points from the $5snh$ - $5sni$ intervals is shown in Fig. 4. Unlike the K splitting plot, the $5sng$ - $5snh$ intervals do not fall anywhere near this line. From the slope we obtain $\alpha_q = [1.1(10) \times 10^3]a_0^5$. Our values for the Sr^+ polarizabilities are given in Table VII. As shown, they are in

TABLE VII. Dipole and quadrupole polarizabilities obtained from this work and other theoretical and experimental results. Note that $\alpha_d^{\text{core}} = 5.81a_0^3$ and $\alpha_q^{\text{core}} = 17a_0^5$ are added if the values do not take account of the Sr^{2+} polarizability [12,17].

$\alpha_d(a_0^3)$	$\alpha_q(a_0^5)$
86(11) ^a	$1.1 \times 10^3(10)$ ^a
89.88 ^b	1346 ^b
97.28 ^c	1651 ^c
93.3 ^d	

^aPresent work.

^bReference [12].

^cReference [19].

^dReference [5].

reasonable agreement with previously determined values, all of which are theoretical.

The analysis of the K splittings gives ionic dipole and quadrupole matrix elements which agree with those of other works. However, this work raises several questions. Is the agreement of the $5sng$ K splitting data with the $5snh$ and $5sni$ data simply fortuitous, or is there a more profound reason? The Sr^+ $\langle 5s|r|5p \rangle$ and $\langle 5s|r^2|4d \rangle$ matrix elements extracted from the K splittings are obviously reasonable. They are due primarily to the l dependence of the splittings, but the n dependence is not consistent. Is there something missing from the model? In addition to the above theoretical questions, these data present an additional theoretical challenge and opportunity. Specifically, we did not use the $5sng$ K splittings or the $5sng$ - $5snh$ intervals because the $5sng$ states are coupled to the $4dnd$ states, which cannot be used in a conventional core polarization analysis. Good theoretically generated $4dnd$ wave functions and energies might allow the $5sng$ data to be used in the analysis, which would certainly improve the results. Nonetheless, in spite of not being able to use the $5sng$ states, we obtain good ionic radial matrix elements and an experimental measurement of the Sr^+ quadrupole polarizability.

It is a pleasure to acknowledge the support of the U.S. Department of Energy, Office of Basic Energy Sciences.

[1] E. S. Shuman and T. F. Gallagher, Phys. Rev. A **74**, 022502 (2006).
 [2] N. Fortson, Phys. Rev. Lett. **70**, 2383 (1993).
 [3] C. Guet and W. R. Johnson, Phys. Rev. A **44**, 1531 (1991).
 [4] J. E. Bernard *et al.*, Phys. Rev. Lett. **82**, 3228 (1999).
 [5] P. S. Barklem and B. J. O'Mara, Mon. Not. R. Astron. Soc. **311**, 535 (2000).
 [6] T. F. Gallagher *et al.*, Phys. Rev. A **26**, 2611 (1982).
 [7] R. A. Komara *et al.*, Phys. Rev. A **67**, 062502 (2003).
 [8] E. L. Snow and S. R. Lundeen, Phys. Rev. A **76**, 052505 (2007).
 [9] J. R. Rubbmark and S. A. Borgström, Phys. Scr. **18**, 196 (1978).

[10] M. A. Baig *et al.*, Chem. Phys. Lett. **296**, 403 (1998).
 [11] M. C. Chidichimo, Phys. Rev. A **38**, 6107 (1988).
 [12] J. Mitroy *et al.*, Phys. Rev. A **77**, 032512 (2008).
 [13] A. Gallagher, Phys. Rev. **157**, 24 (1967).
 [14] A. Burgess and V. B. Sheorey, J. Phys. B **7**, 2403 (1974).
 [15] E. Biémont *et al.*, Eur. Phys. J. D **11**, 355 (2000).
 [16] A. Lindgard and S. E. Nielsen, At. Data Nucl. Data Tables **19**, 533 (1977).
 [17] J. Mitroy and M. W. J. Bromley, Phys. Rev. A **68**, 052714 (2003).
 [18] E. L. Snow and S. R. Lundeen, Phys. Rev. A **75**, 062512 (2007).
 [19] S. H. Patil and K. T. Tang, J. Chem. Phys. **106**, 2298 (1997).